Science Advances
AAAS

advances.sciencemag.org/cgi/content/full/7/6/eabd7013/DC1

Supplementary Materials for

Scalable representation of time in the hippocampus

Akihiro Shimbo, Ei-Ichi Izawa, Shigeyoshi Fujisawa*

*Corresponding author. Email: shigeyoshi.fujisawa@riken.jp

Published 3 February 2021, *Sci. Adv.* **7**, eabd7013 (2021)
DOI: 10.1126/sciadv.abd7013

This PDF file includes:

Supplementary Table

Table S1. Basic physiology statistics

A. Total pyramidal cells and time cells in each task

	Task 1 (Figures 1,2,3,4)	Task 2 (Figure S2)	Task 3 (Figure S3)	Task 4 (Figure 5)
Rats	s15, s18, s20, s23, s26, s32, s39	s25, s28, s33	s30, s34, s36	s26, s32, s39
Total sessions	45	16	15	13
Total pyramidal cells [1)]	2041	1276	818	1063
Total time cells [2)]	454	241	61	238

B. Number of pyramidal cells in each session

	Task 1							Task2			Task3			Task4		
Session# \ Rat#	s15	s18	s20	s23	s26	s32	s39	s25	s28	s33	s30	s34	s36	s26	s32	s39
1	19	63	57	34	49	38	59	73	90	91	113	56	70	59	57	76
2	22	62	59	30	56	34	48	75	89	88	48	32	55	45	40	80
3	25	56	65	37	48	36	55	70	86	86	39	35	58	76	73	
4	28	39	72	47	53			70	99	84	80	35	46	75	71	
5	18		64		35			47	86	90	66	44	41		82	
6	24		75		42			52							77	
7	34		70												72	
8	21		66												97	
9	27		62												83	
10	20		43													
11	29		52													
12	37		64													
13			67													

C. Number of time cells in each session

	Task 1							Task2			Task3			Task4		
Session# \ Rat#	s15	s18	s20	s23	s26	s32	s39	s25	s28	s33	s30	s34	s36	s26	s32	s39
1	4	9	20	7	11	8	16	8	9	11	1	5	4	7	12	9
2	3	12	21	6	12	14	8	22	18	14	2	3	3	6	12	9
3	9	4	22	6	5	8	14	22	12	17	1	2	9	11	19	
4	6	9	19	10	5			19	17	11	5	2	13	11	24	
5	3		14		3			16	13	26	2	1	8		23	
6	5		27		8			6							28	
7	7		17												18	
8	4		24												24	
9	5		7												25	
10	3		10													
11	5		11													
12	5		13													
13			15													

1) The classification method of putative pyramidal cells was described in Figure S1C.

2) The classification method of time cells is described in Methods.

Supplementary Figures

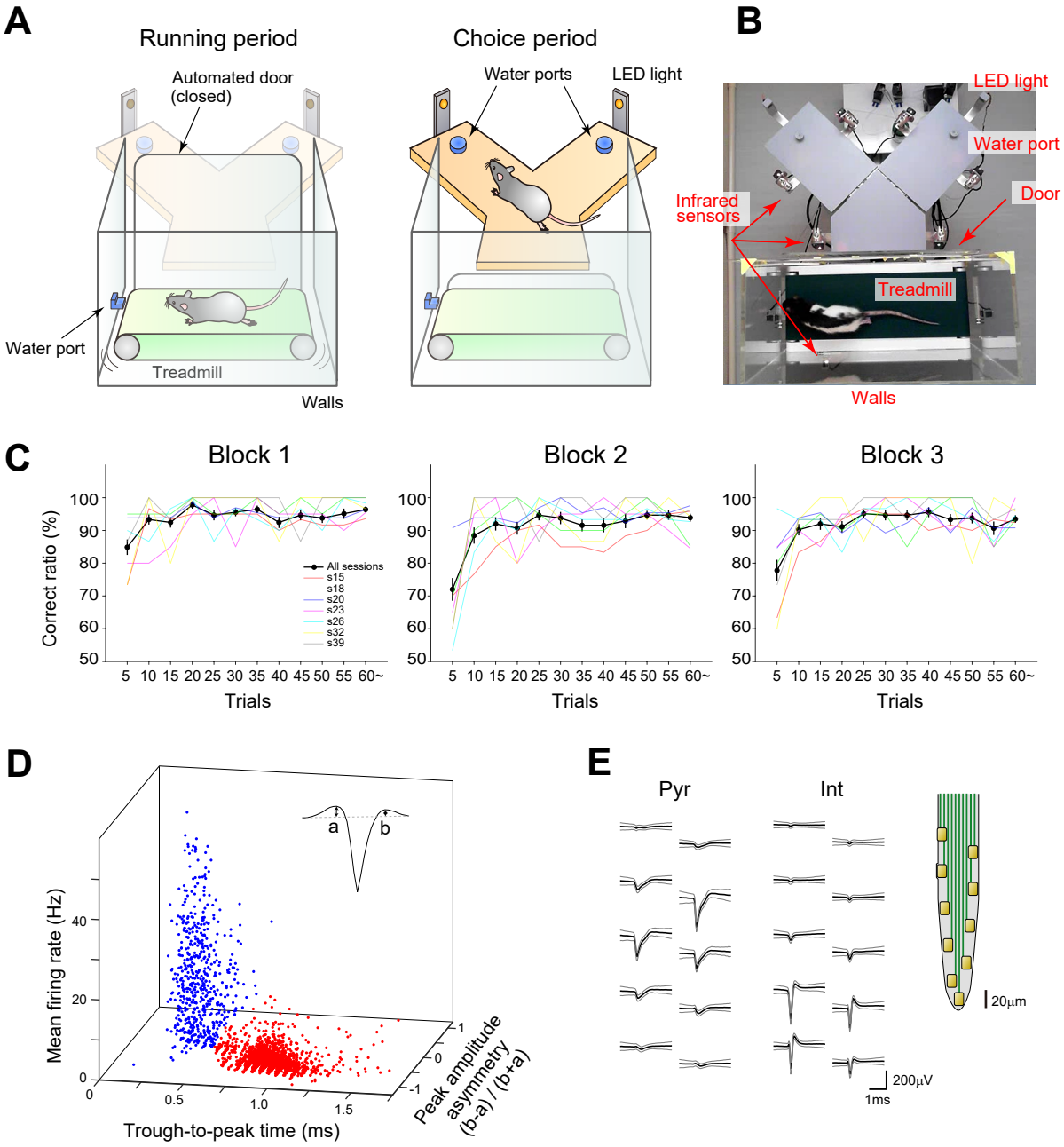

Fig. S1. Experimental apparatus and unit classification methods. (A) Schematics of behavioral experimental apparatus for the tasks. **(B)** Photograph of the experimental apparatus. Photo Credit: Akihiro Shimbo, RIKEN Center for Brain Science. **(C)** Behavioral performance across trials in each block in the temporal bisection task with the standard-extended-standard block paradigm (Task1). The performances of every 5 trials were averaged in all sessions for all animals (black lines, Mean ± S.E.M) or individual animals (colored lines). **(D)** Classification of units into putative pyramidal neurons and interneurons, with using the mean firing rates and shapes of the waveforms. Red and blue dots indicate the units classified into putative pyramidal neurons and interneurons, respectively. **(E)** Representative waveforms of a putative pyramidal neuron and interneuron. Thick lines indicate mean traces and thin lines indicate standard deviations. Inset indicates channel alignment of one shank (10 channels) of a silicon probe. Thick lines indicate the mean traces, and thin lines indicate standard deviations.

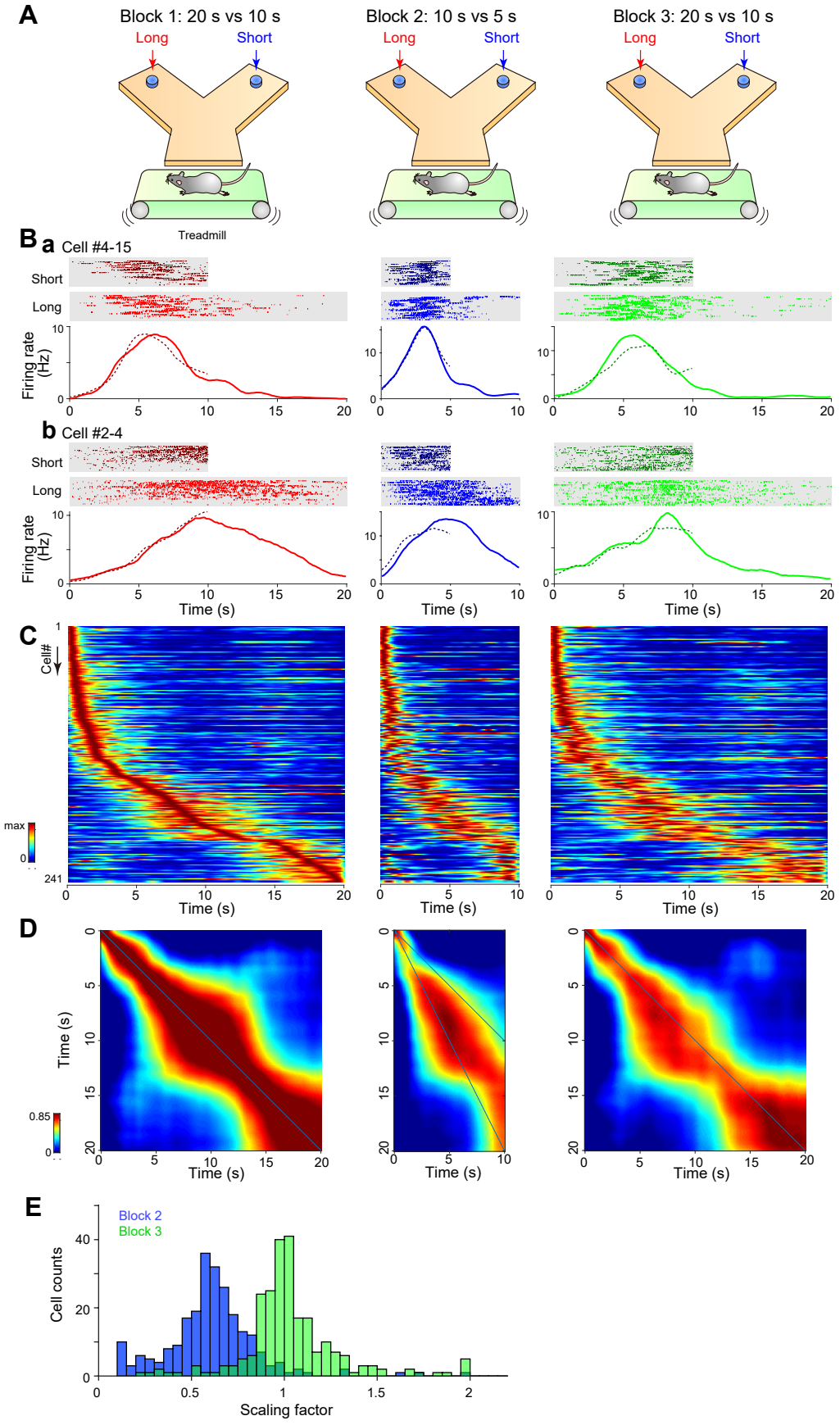

Fig. S2. Scalable time representation of CA1 neurons in the temporal bisection task with standard-contracted-standard block paradigm.

Fig. S2. Scalable time representation of CA1 neurons in the temporal bisection task with standard-contracted-standard block paradigm. (A) Schematic of the task (Task 2). The experimental procedures used during the single trials were the same as those used during Task 1. The sets of interval times to bisect were contracted down and back across the blocks. In Blocks 1 and 3, the sets of interval times to discriminate between were 20 s (long) and 10 s (short). In Block 2, the sets of interval times were 10 s (long) and 5 s (short). **(B a-b)** Firing patterns of two representative time cells in Blocks 1 (left column), 2 (center), and 3 (right). Top, raster plots of short and long interval trials. Bottom, PETHs of long (solid line) and short (dotted line) interval trials. The classification method of time cells is described in the main text and Methods. **(C)** Firing patterns of time cells in Blocks 1 (left), 2 (center), and 3 (right) (n = 241 units from 3 rats). Each row represents the PETH of a single neuron during long interval trials in each block. The color scale represents the firing rate of each neuron (red represents the maximum firing rate of each neuron and blue represents 0 Hz). The neurons were ordered according to the time of their peak firing rates in Block 1. **(D)** Population vector analyses of the data (C). Left, auto-correlation of the population vector matrix of the time cells of Block 1. Center, cross-correlation of the population vector matrices of Blocks 1 and 2. Right, cross-correlation of the population vector matrices of Blocks 1 and 3. **(E)** The distributions of the scaling factors of the time cells between Block 1 and 2 (blue) and Block 1 and 3 (green).

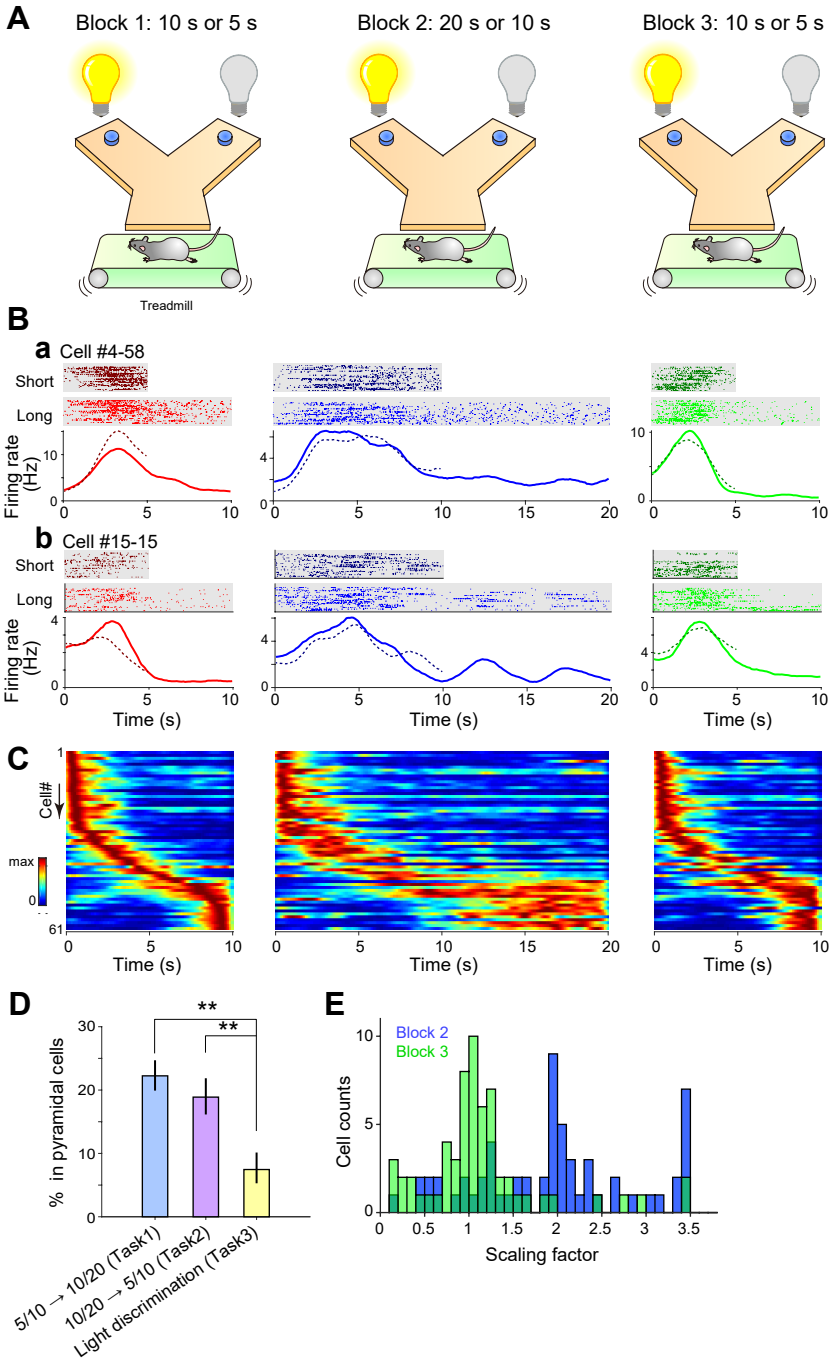

Fig. S3. Scalable time representation of CA1 neurons in the light discrimination task. (A) Schematic of the task (Task 3). The rats ran on a treadmill for long or short intervals of time. After the forced running, the rats were required to select the left or right arm of the Y-maze in a light-guided manner. The interval times were not relevant to the rewarded arm. The block paradigm was the same as that used in Task 1. **(B a-b)** Firing patterns of two representative time cells in Blocks 1 (left column), 2 (center), and 3 (right). Top, raster plots of short and long interval trials. Bottom, PETHs of long (solid line) and short (dotted line) interval trials. The classification method of time cells is described in the main text and Methods. **(C)** Firing patterns of time cells in Blocks 1 (left), 2 (center), and 3 (right) (n = 61 units from 3 rats). Each row represents the PETH of a single neuron during long interval trials in each block. The color scale represents the firing rate of each neuron (red represents the maximum firing rate of each neuron and blue represents 0 Hz). Neurons were ordered according to the time of their peak firing rates in Block 1. **(D)** Ratios of the time cells to the pyramidal cells in Tasks 1, 2, and 3. Clopper-Pearson exact confidence intervals (**P < 0.01) are used in (D) & (E). Bars indicate a 99% confidence interval. **(E)** The distributions of the scaling factors of time cells between Block 1 and 2 (blue) and Block 1 and 3 (green) in Task 2.

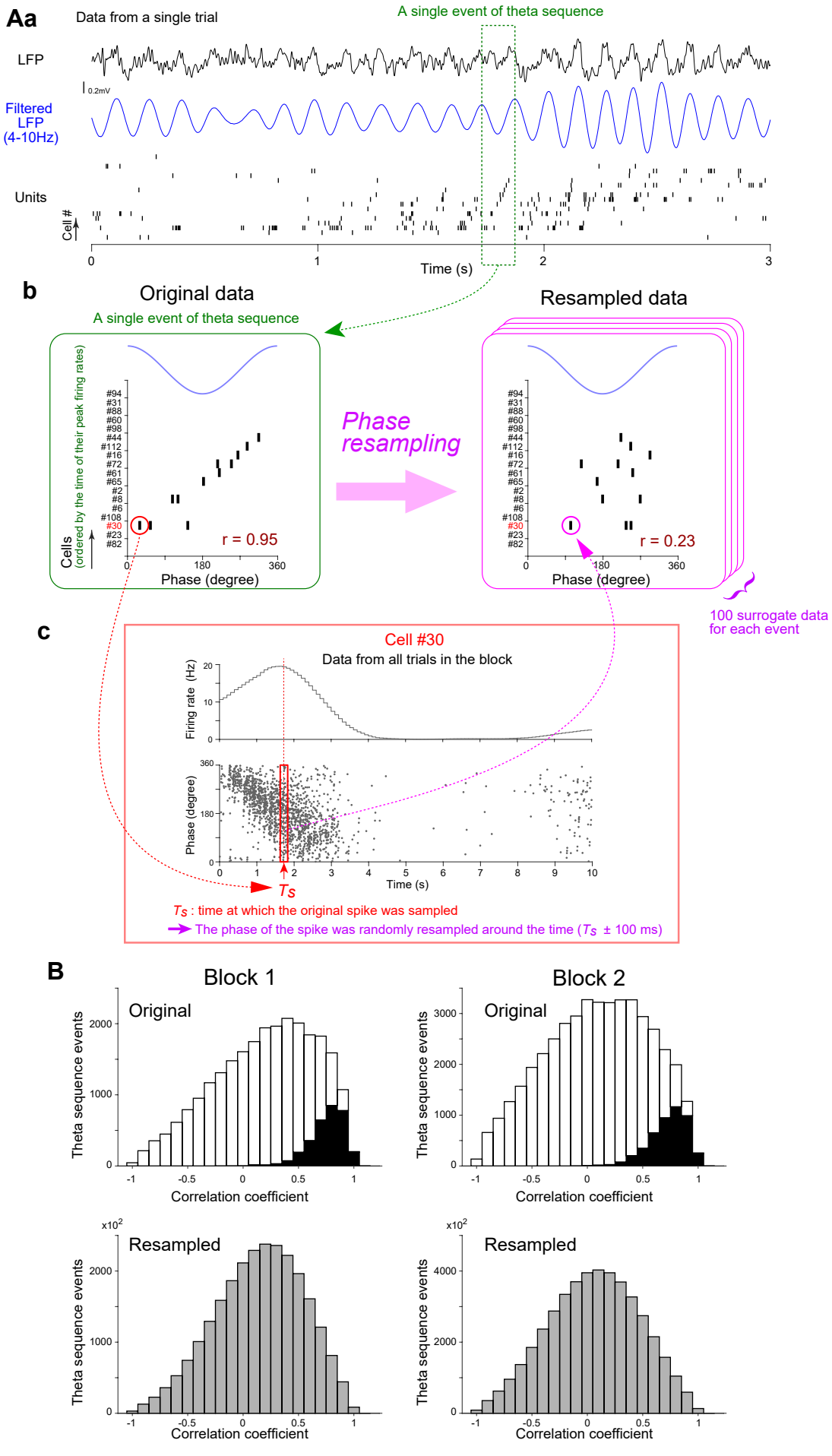

Fig. S4. Theta sequences of time cells have higher correlative structures than those predicted from phase precession.

Fig. S4. Theta sequences of time cells have higher correlative structures than those predicted from phase precession. (A) Schematics of the phase resampling method. We analyzed theta sequence events in which more than 3 neurons were activated in single theta cycles. An example single theta sequence in a single trial was shown in **(a)**. Here, we constructed a surrogate event while preserving the distributions of phase precession of individual neurons **(b)**. First, we prepared a phase-time plot of each neuron from the data of all trials in the block **(c)**. Then, to construct a surrogate event, the phase of each spike of each neuron in the original event was randomly resampled from the phase-time plot of the neuron in the time bin between Ts – 100 ms and Ts +100 ms, where Ts is the time when the spike occurred (**b, c**). We repeated this 100 times for each original theta sequence. We then assessed the correlation coefficients between the spiking phases (x-axis in **b**) and the cell order (y-axis in **b**) of the original and surrogate events. If the correlation of the original event was higher than the 5% rank of the surrogate ones, we considered that the theta sequence possesses a significantly higher correlation than that predicted from individual phase precession. **(B)** The distribution of correlations of original (top) and resampled (bottom) theta sequence events in Blocks 1 (left) and 2 (right). The events with significant correlations are indicated in black (12.6% in Block 1 and 10.5% in Block 2). As the group data, the ratios of events with significant correlations were significantly higher than chance level (Clopper-Pearson confidence intervals for 99%, CI = 12.0% to 13.1% in Block 1, CI = 10.1% to 10.9% in Block 2; chance level is 5%). n=25256 events in Block 1 and 44667 events in Block 2.